The semiannual oscillation of the tropical zonal wind in the middle atmosphere derived from satellite geopotential height retrievals

Anne K. Smith[1], Rolando R. Garcia[1], Andrew C. Moss[2], Nicholas J. Mitchell[2]

1. Atmospheric Chemistry Observations and Modeling, National Center for Atmospheric Research, Boulder Colorado, USA

2. Centre for Space, Atmospheric and Oceanic Science, University of Bath, Bath, UK

Corresponding author address: Anne K. Smith, Atmospheric Chemistry Observations and Modeling, National Center for Atmospheric Research, Boulder, CO USA 80301;

email: aksmith@ucar.edu; phone: 303-497-1876

Abstract

The dominant mode of seasonal variability in the global tropical upper stratosphere and mesosphere zonal wind is the Semi-Annual Oscillation (SAO). However, it is notoriously difficult to measure winds at these heights from satellite or ground-based remote sensing. Here we use the balance wind relationship to derive monthly and zonally averaged zonal winds in the tropics from satellite retrievals of geopotential height. Data from the Aura Microwave Limb Sounder (MLS) cover about 12.5 years and those from the TIMED Sounding of the Atmosphere using Broadband Emission Radiometry (SABER) cover almost 15 years. The derived winds agree with direct wind observations below 10 hPa and above 80 km; there are no direct wind observations for validation in the intervening layers of the middle atmosphere. The derived winds show the following prominent peaks associated with the semiannual oscillation (SAO): easterly maxima near the solstices at 1.0 hPa, westerly maxima near the equinoxes at 0.1 hPa, and easterly maxima near the equinoxes at 0.01 hPa. The magnitudes of these three wind maxima are stronger during the first cycle (January at 1.0 hPa and March at 0.1 and 0.01 hPa). The month and pressure level of the wind maxima shift depending on the phase of the QBO at 10 hPa. During easterly QBO, the westerly maxima are shifted upward, are about 10 m s^{-1} stronger, and occur approximately one month later than those during the westerly QBO phase.

41 **1. Introduction**

42 The semi-annual oscillation (SAO) in zonal wind is the dominant mode of
43 seasonal variability in the tropical middle atmosphere between the middle stratosphere
44 and the upper mesosphere. The current picture of the SAO is constructed from combining
45 various historical and more recent sets of *in situ* and remote observations. Rocket wind
46 measurements (e.g., Hirota, 1978; Garcia et al., 1997) and analyses of conventional
47 meteorological data (Baldwin and Gray, 2005; Rienecker et al., 2012) show an SAO in
48 the upper stratosphere. However, there are substantial differences in the tropical winds in
49 the upper stratosphere between several commonly-used climatologies (Randel et al,
50 2004). Wind observations from satellite (Garcia et al., 1997) and radar (e.g.,
51 Venkateswara Rao et al., 2012; Davis et al., 2012) also show an SAO in tropical zonal
52 winds in the upper mesosphere.

53 Several decades of observations by research satellites have greatly increased the
54 knowledge and understanding of the middle atmosphere. Satellite observations have the
55 benefits of near global coverage and good continuity in time. Middle atmosphere winds
56 were observed by HRDI (High Resolution Doppler Interferometer) on UARS (Upper
57 Atmosphere Research Satellite) in the stratosphere and mesosphere. Garcia et al. (1997)
58 and Ray et al. (1998) show the SAO from these data over the altitude ranges 10-40 km;
59 Garcia et al. (1997) also include HRDI observations at 65-110 km. More recently, TIDI
60 (TIMED Doppler Interferometer) on TIMED (Thermosphere, Ionosphere, Mesosphere
61 Energetics and Dynamics) measured winds for altitudes above 60 km; TIDI data have
62 been used mainly to investigate wave phenomena rather than zonally averaged winds

63 because of uncertainty in quantifying spacecraft effects that impact the determination of
64 the absolute geophysical wind (Niciejewski et al., 2006).
65 Satellite direct wind measurements have never been available in the upper
66 stratosphere and lower to middle mesosphere. With such a gap, the connection between
67 the SAO in the mean winds at the stratopause and that in the upper mesosphere has not
68 been well constrained by observations. In addition, there has been little observational
69 investigation of the variation of the SAO in relation to other dynamical phenomena such
70 as the quasi-biennial oscillation (QBO) and extratropical dynamical variability. With the
71 increasing awareness of coupling of atmospheric dynamical processes across different
72 vertical levels and latitudinal regions, there is a need for studies that characterize the
73 SAO and its variability.
74 In this study, we present tropical mesospheric winds derived from the temperature
75 measurements made by the Sounding of the Atmosphere using Broadband Emission
76 Radiometry (SABER) instrument on the TIMED satellite and the Microwave Limb
77 Sounder (MLS) instrument on the Aura satellite and we assess their reliability in the
78 lower stratosphere and upper mesosphere. Although observed profiles from both
79 instruments span the entire middle atmosphere and SABER profiles even extend into the
80 lower thermosphere, the range investigated here is limited to altitudes below about 84 km
81 (0.004 hPa); at higher altitudes, the limited vertical resolution of MLS, and potential
82 contamination by the diurnal tide for both instruments, make determination of zonal-
83 mean zonal winds problematic. The long duration of the measurement records, which
84 currently exceed a dozen years for MLS and approaches 15 years for SABER, allows us

to investigate the interannual variability of the SAO and the relationship between it and the QBO.

2. Data and Processing

2.1 TIMED/SABER geopotential height data

Temperature profiles are retrieved from SABER Version 2.0 measurements of CO_2 emission. Remsberg et al. (2008) describe the temperature retrieval and uncertainties from Version 1.07. Updated uncertainty information for Version 2.0 is available from http://saber.gats-inc.com/temp_errors.php. The uncertainty due to precision of single temperature profiles over the altitude range 20-80 km is less than 1.8 K. For the standard data products, temperature profiles are integrated using the hydrostatic relation to determine geopotential height thicknesses; heights are then assigned by tying onto daily NCEP (National Center for Environmental Prediction) analyses at 10 hPa. In this study, we use the altitude and pressure data from the SABER Level2A Version 2.0 files for the period 25 January 2002 through 31 December 2016, available from http://saber.gats-inc.com.

Level 2A SABER profiles are obtained from observations made at variable latitudes along the tangent path of the observations over a range of pressure. For the analysis carried out here, the data are sorted into bins with a width of 4° in latitude. All profiles along one leg of an orbit that fall into a latitude bin are averaged to produce a mean profile for that bin; the profile coordinates are then the average longitude and time of the profiles included in the average. The effective vertical resolution of the SABER data is 0.3 scale heights; the scale height is the ratio ln $(p_0 \,/\, p)$, where p_0 is a reference

pressure. A vertical resolution of 0.3 scale heights is equivalent to 2.1 km, assuming a mean scale height H = 7 km for the middle atmosphere. The lower limit of the analysis is 70 hPa; below this level, increasing noise and data gaps make the results less reliable.

Due to the precession of the TIMED satellite, the local time of SABER observations shifts from day to day. For any given day, the local times sampled have two narrow ranges that, at the equator, are about 8.8 hours apart. The TIMED satellite executes a yaw maneuver about every 60-65 days on an annually repeating schedule. Near-complete local time coverage is obtained during each yaw cycle. A gap in local time coverage occurs near noon at all latitudes and times of the year; at the equator the gap extends for about 2 hours.

2.2 Aura/MLS geopotential height data

Schwartz et al. (2008) describe the retrieval and validation of MLS geopotential height data. Geopotential height profiles from MLS Version 4.2 are available from http://disc.sci.gsfc.nasa.gov/Aura/data-holdings/MLS/index.shtml. See http://mls.jpl.nasa.gov/data/v4-2_data_quality_document.pdf for an updated discussion of the data quality, screening recommendations, and uncertainties in the geopotential height data. The available data from 2 August 2004 to 31 December 2016 are used in the present study. The thicknesses of atmospheric layers are determined from the temperature and then tied to the height at 100 hPa determined from spacecraft pointing information.

The MLS data are given at fixed pressure levels with resolution that varies with altitude: 12 pressure levels from 100 to 10 hPa and from 10 to 1 hPa; 6 pressure levels from 1 to 0.1 hPa; and three pressure levels from 0.1 to 0.01 hPa. Geopotential height

131 data above 0.01 hPa are not recommended for use; data at 0.01 hPa proved to be too
132 noisy for wind calculations at the equator and are not used in the present analysis. The
133 data at the MLS geopotential height levels are used with no additional interpolation in
134 pressure. Sampling in latitude is regular and is approximately every 1.5 degrees in
135 latitude in the tropical and subtropical region. The latitude bins used in the analysis here
136 conform to this natural resolution, and are at 1.5° intervals.
137 After screening for data quality, precision, data status, and data convergence, as
138 described in the MLS documentation, outliers were still found that perturbed the wind
139 calculations. Additional screening removed points that were outside the normal height
140 dependent range; the approximate quantity of data points removed was 0.01%.
141
142 *2.3 Time-series analysis*
143 In the upper mesosphere, tidal amplitudes become large so special care is needed
144 to separate the migrating diurnal tide from the SAO. The amplitude of this tide has large
145 semiannual variations (e.g. Burrage, 1995a; Wu et al., 2008; Davis et al., 2013). Since
146 SABER and MLS geopotential height data are available twice per day and have very low
147 rates of missing profiles, the asynoptic mapping method described by Salby (1982a;
148 1982b) can be used to separate the diurnal tidal variations from the variations in the
149 background.
150 In principle, the asynoptic sampling analysis technique applied to SABER profiles
151 can give a clean separation of the diurnal tidal period of 1 day and the SAO period of
152 about 183 days (see discussion and verification by Salby, 1982a). However, as noted
153 above, the sampling of SABER profiles is not uniform; there is a small shift to the track

154 of limb viewing points about every 60-65 days as TIMED executes a yaw maneuver. In
155 our analysis, we shift the coordinates of the profiles slightly to conform to a regular
156 sampling pattern that is midway between the profile locations for the left-viewing and
157 right-viewing periods. Tests with synthetic data show that this shift causes the diurnal
158 tide to contaminate the zonal-mean time-mean geopotential height and hence onto the
159 calculated zonal wind. At higher altitudes where the amplitude of the tide in temperature
160 and geopotential height is large, this introduces a bias in the time mean wind.
161 Comparison of the SABER winds derived in this study with radar observations indicate
162 systematic differences that are small but not negligible at 80 km (~0.01 hPa) and grow
163 with altitude. The biases fit the characteristics of tidal contamination found in our tests
164 with synthetic data, and appear to be confined to the long-term average background mean
165 wind, as predicted by these tests. Note that the amplitude of the migrating semidiurnal
166 tide also grows in the upper mesosphere (e.g., Burrage et al., 1995b; Pancheva et al.,
167 2009) but it is not expected to reach large enough amplitude to have a major impact on
168 the tropical wind calculations over the height range considered here.
169 Aura is in a sun-synchronous orbit and the MLS data sampling is regular in
170 longitude and time. The asynoptic sampling is therefore applied to the MLS profiles
171 without any need for adjusting the locations and times of the profiles. The MLS analysis
172 allows us to isolate fields at frequencies lower than 1 day that are free from
173 contamination by the diurnal tide (Salby, 1982a). In other words, the diurnal tide and its
174 variability should not cause any contamination of the MLS zonal and time mean
175 geopotential heights. The amplitudes of the semidiurnal tide and other tidal frequencies
176 are not large enough to affect the analysis in the equatorial lower and middle mesosphere.

177 Because of the tidal contamination, we restrict SABER analysis to altitudes below
178 0.004 hPa (about 84 km). As discussed below, the zonally averaged zonal winds at this
179 cutoff altitude agree well with observations if the multiyear time mean wind is removed.
180
181 *2.4 Determining winds from geopotential height*
182 The relationship between large scale zonal wind and geopotential can be
183 determined from the meridional momentum equation:

184 $$\frac{\partial v}{\partial t} + \frac{u}{a\cos\varphi}\frac{\partial v}{\partial \lambda} + \frac{v}{a}\frac{\partial v}{\partial \varphi} + w\frac{\partial v}{\partial z} + fu + \frac{u^2}{a}\tan\varphi = -\frac{1}{a}\frac{\partial \Phi}{\partial \varphi} \qquad (1)$$

185 u, v, and w are zonal, meridional, and vertical wind components, λ and φ are longitude
186 and latitude, z is log-pressure altitude, f is the Coriolis parameter, a is the Earth radius,
187 and Φ is the geopotential. Taking the zonal mean (overbar), expressing eddy quantities
188 (primed) in flux form, and neglecting zonal mean v and w gives

189 $$\frac{\bar{u}^2}{a}\tan\varphi + f\bar{u} + \frac{1}{a}\frac{\partial \bar{\Phi}}{\partial \varphi} + \left(\frac{1}{a\cos\varphi}\frac{\partial \overline{v'v'}\cos\varphi}{\partial \varphi} + \frac{1}{\rho}\frac{\partial \rho\overline{v'w'}}{\partial z}\right) = 0 \qquad (2)$$

190 D. Ortland (personal communication, 2017) found that the eddy flux terms in parentheses
191 could not be neglected in the tropical upper mesosphere where the migrating diurnal tide
192 reaches large amplitude. This is another reason why we do not extend the current analysis
193 into the upper mesosphere. Lower in the middle atmosphere, where the tidal meridional
194 winds can be neglected, Eq. (2) reduces to

195 $$\frac{\bar{u}^2}{a}\tan\varphi + f\bar{u} + \frac{1}{a}\frac{\partial \bar{\Phi}}{\partial \varphi} = 0 \qquad (3)$$

196 Randel (1987) showed that Eq. (3) gave good results for middle atmosphere zonal mean
197 zonal wind; this is the formula we use in this study. In practice, the first term is quite

198 small near the equator so, in effect, solving Eq. (3) yields geostrophic winds there. The
199 geopotential is obtained from the geopotential height data simply by multiplying by *g*, the
200 acceleration of gravity, which we take to be equal to its value at sea level.

201 The main limiting factor of applying Eq. (3) close to the equator is that even small
202 errors in the geopotential height data can introduce large errors in the zonal wind. This is
203 because the meridional variation of $\overline{\Phi}$ is very slight near the Equator, so its gradient is a
204 (small) difference of two large numbers. On the other hand, errors in the data are random,
205 such that their contribution to the calculated geopotential gradient becomes increasingly
206 larger relative to the true gradient as the Equator is approached. Observations from both
207 SABER and MLS have very few data gaps. Sampling in a specified latitude interval
208 includes about 30 profiles per day and 900 profiles per month. The excellent precision
209 and large number of profiles of both of the satellite datasets means that noise is
210 manageable in the calculations except very close to the Equator, as discussed below.

211 For both data sets, we compute the spectra of geopotential height using the
212 asynoptic sampling method over the entire time period: almost 15 years for SABER and
213 more than 12 years for MLS. We then synthesize the spectral results for low frequency
214 variations (periods from 100 days to infinity) to get daily geopotential height profiles at
215 each latitude band and day. These are averaged for each month. The monthly
216 geopotential height data for MLS are smoothed in latitude using a 5-point averaging. Due
217 to the smoothing inherent in the binning of profiles that are irregularly spaced in latitude,
218 no additional latitudinal smoothing is used for the SABER geopotential heights. The
219 zonal wind values at all latitudes except those very close to the equator come from Eq.
220 (3).

221 For the results shown here, the equatorial and near equatorial winds were
222 estimated by cubic spline interpolation of the balance winds obtained from Eq. (3) at and
223 poleward of latitudes of ±8° for SABER and ±6° for MLS. We experimented with many
224 options before settling on these choices of how much latitudinal smoothing to apply to
225 each dataset and how close to the equator to carry the balance wind calculations. The
226 basic magnitude and structure of the wind was not highly sensitive to the details of the
227 calculations. The method used gave the best overall agreement of the equatorial winds
228 derived from MLS and SABER with each other and with the correlative data presented
229 below.
230 Figure 1 shows the background time mean wind calculated from SABER and
231 MLS. The two agree very well up to 0.04 hPa. One exception is at 1 hPa, where the
232 SABER analysis indicates the wind is weak easterly while the MLS analysis gives a weak
233 westerly wind. The large magnitudes in the SABER mean wind above 0.01 hPa are
234 consistent with tidal aliasing, as discussed above. Although tidal aliasing could contribute
235 to the discrepancy between the SABER and MLS wind estimates above 0.06 hPa, it is
236 also possible that a portion of the discrepancy is due to the coarser vertical resolution and
237 increasing noise in the MLS observations.
238 In all subsequent figures that show SABER winds, the multi-year time-average
239 wind is removed above 0.03 hPa. This pressure cutoff is chosen for three reasons: 1) it is
240 approximately the level where the migrating diurnal tide becomes sufficiently large to
241 contaminate the zonal mean wind, 2) the winds estimated from SABER and MLS
242 increasingly diverge above this level, and 3) the SABER estimate for the time-average

243 wind is small at this pressure level so removal of the mean does not introduce a
244 discontinuity in the vertical dimension.
245
246 *2.5 Comparison with direct wind measurements from radiosonde*
247 As noted in the Introduction, the vertical range for which there are direct wind
248 observations in the tropical middle atmosphere is limited. For validation of the SABER
249 and MLS wind analyses, we are particularly interested in long-term observations since
250 February 2002. Here, we compare the satellite winds with two available data sets, one in
251 the lower stratosphere and the other in the upper mesosphere.
252 The monthly mean radiosonde winds at Singapore (1°N; 104°E) in the lower
253 stratosphere are included in a widely used dataset made available by the Free University
254 of Berlin at http://www.geo.fu-berlin.de/en/met/ag/strat/produkte/qbo/; see Naujokat
255 (1986) for a description of the data. The variability of the stratospheric equatorial wind
256 on monthly or longer timescales is dominated by the QBO. Figure 2 shows a comparison
257 of the Singapore winds at levels near 10, 20, 30 and 45 hPa with the monthly averaged
258 zonal mean winds at the same or nearby pressures determined from SABER and MLS.
259 SABER winds are not shown at 10 hPa because this is the geopotential height tie-on
260 level; geopotential heights at 10 hPa in the SABER data come from the NCEP analysis.
261 The winds from both satellite analyses follow the phase of the QBO quite well but
262 there are some differences that stand out. SABER winds indicate a similar QBO
263 magnitude to the radiosonde winds and to the winds derived from MLS at 30 and 45 hPa
264 but the westerly maxima are systematically weaker at 20 hPa. This may be due to the
265 coarser latitudinal resolution of the SABER data since the westerly phase of the QBO is

narrowly confined to the deep tropics. The month-to-month variability does not always agree. The satellite winds show more month-to-month variability during periods of strong westerly wind; both the satellite and Singapore winds are variable during periods of strong easterly wind. There could also be a systematic discrepancy between zonally averaged satellite winds and single-longitude radiosonde winds arising from zonal asymmetries in the QBO (see, e.g., Hamilton et al., 2004; Kawatani et al., 2016) that are not captured in the Singapore observations.

2.6 Comparison with direct wind measurements from meteor radar

Wind data spanning 2002-2007, with some gaps, were taken by a meteor radar at Ascension Island (8°S; 14°W) and are described by Davis et al. (2013) and Moss et al. (2016). The Ascension Island meteor radar is a commercially-produced standard Skiymet system and operated in an all-sky configuration with a peak power of 12 kW up until 2007 transmitting at a frequency of 43.5 MHz. The data used in this study cover the period January 2002 to December 2007.

Mesospheric winds were calculated from these data in the same way as previous studies (e.g. Davies et al., 2013; Moss et al., 2016). To calculate the atmospheric mean winds, the data are binned into six height gates at 78-83 km, 83-86 km, 86-89 km, 89-92 km, 92-95 km, and 95-100 km. The lowermost and uppermost height gates are wider to allow enough meteor observations to make accurate measurements. Coverage over all local times allows for the separation of tidal winds from the background daily means. A least-squares method is used to determine the magnitude and direction of the mean wind,

288 which is then split into zonal and meridional components. Low-pass filtering is applied to
289 produce the 31-day monthly mean-wind estimates.
290 Figure 3 compares the monthly mean winds from Ascension Island with the
291 SABER derived zonal-mean winds at 8°S for the same period. MLS winds are not shown
292 because these altitudes are above the recommended pressure range of MLS geopotential
293 height data. For these comparisons, the SABER wind values were interpolated onto
294 altitude levels.
295 As noted above, diurnal tides can alias into the time mean wind in the SABER
296 analysis. The altitude levels shown in Figure 3 are above 0.03 hPa so the time mean has
297 been removed from the SABER winds as discussed in Section 2.4. At the lowest level
298 shown (81 km), the magnitude, timing, and interannual variability of the SABER wind
299 variations agree fairly well with the radar. Variations are also similar at the next higher
300 level (84 km). For both datasets, the dominant period of variability is semiannual. At
301 levels above 84 km, major discrepancies appear. For this reason, we limit the further
302 analysis of SABER winds to levels below 0.004 hPa, approximately 84 km.
303
304 **3. Climatological SAO**
305 Figure 4 shows the climatological monthly average zonal-mean zonal wind from
306 SABER and MLS at the equator for February 2002-May 2016. The tropical SAO near the
307 stratopause (1 hPa, 50 km) is characterized by easterly wind maxima at the solstices. The
308 easterly peaks are stronger in NH winter (December-January). Following both solstice
309 periods, the SAO easterly winds descend downward to about 10 hPa, where the QBO also
310 has large amplitude (not apparent in the multiyear average, which effectively removes the

311 QBO). The timing and magnitudes of the wind variations are similar in the analyses from
312 the two datasets but there are some differences. One difference is that the MLS winds at
313 all levels are more westerly during June-August (weaker easterlies at 1 hPa and stronger
314 westerlies at 0.1 hPa). The difference in the time-mean wind at 1 hPa (see Figure 1) is
315 associated with stronger westerly winds in April-May and weaker easterly winds in July-
316 August in the MLS analysis.

317 Holton and Wehrbein (1980) proposed that the solstice easterly winds of the SAO
318 at the stratopause could be attributed in part to the advection of zonal-mean easterly
319 momentum across the equator by the Brewer-Dobson circulation. The upper branch of
320 this circulation flows from the summer to winter hemisphere and is strong in the upper
321 stratosphere, giving two periods of easterly acceleration, as easterly zonal-mean zonal
322 winds are advected from the summer to the winter hemisphere during the Northern and
323 Southern Hemisphere summers. The easterlies could also have contributions from
324 momentum transfer by planetary waves in the winter hemisphere (Hopkins, 1975). The
325 presence of westerly winds during equinox periods indicates wave driving of the zonal
326 wind; angular momentum conservation dictates that these winds cannot be caused by
327 advection by the mean meridional circulation. The westerly winds appear to propagate
328 downward from 0.1 to about 3 hPa.

329 The SAO dominates the seasonal variability of equatorial winds from the upper
330 stratosphere to the upper mesosphere. Above the stratopause, the SAO signal is defined
331 by equinoctial maxima of westerly winds peaking near 0.1 hPa and easterly winds
332 peaking near 0.01 hPa. Dunkerton (1982) proposed that the SAO winds near the

stratopause would selectively filter eastward or westward gravity waves that would then drive an SAO of opposite phase when they dissipated in the upper mesosphere.

Figure 5 shows latitude-month cross-section of the winds at 0.9-1.0, 0.15, and 0.014 hPa, which correspond to the easterly and westerly SAO peaks in the lower mesosphere in Figure 4 and the easterly peak in the upper mesosphere (SABER only). The wind cross-sections from MLS and SABER at 0.9-1.0 hPa are very similar to each other. The wind pattern is qualitatively consistent with the generation of the SAO easterly phase by advection; easterly winds in the summer hemisphere extend into the tropics. On the other hand, westerly winds are evident during the equinox season, which suggests wave forcing at that time. The pattern at 0.15 hPa (middle panels; the level of the westerly wind SAO maxima) is similar in structure to that at the stratopause (lower panels). However, note that the equatorial time-mean wind at this level is westerly. The downward propagation of the westerly maxima seen in Figure 4 is consistent with a feature driven by waves interacting with the mean zonal wind. The MLS-SABER difference during June-August noted in the discussion of Figure 4 can also be seen in Figure 5.

The SAO easterly wind peaks at 0.014 hPa in Figure 5 are qualitatively somewhat different from those below. They show a connection to easterly features at higher latitudes of either hemisphere, in common with the appearance at lower levels. However, they also show maxima confined to low latitudes. Easterly winds appear near the equator in March-April, disappear during the solstice months, and then weaker easterly winds reappear in September-October. Dunkerton (1982) proposed that critical level filtering of gravity waves by the winds in the stratopause SAO would affect the waves reaching the

upper mesosphere. When these gravity waves dissipate, they would drive an SAO that was out of phase with that below. The wind results shown in Figures 4 and 5 are somewhat consistent with this explanation. However, instead of seeing alternating easterly and westerly wind maxima at the stratopause (~1.0 hPa) as assumed by Dunkerton (1982), the westerly wind maxima occur at a higher altitude.

4. Variability of the SAO and its Relationship to the QBO

Figures 6 and 7 show timeseries of the equatorial wind for the entire period derived from SABER and MLS, respectively. It is evident that there is substantial variability in the magnitudes of the wind extremes and the altitudes and months at which the minima and maxima occur. For most cycles, the MLS and SABER winds show similar behavior in the magnitude, timing, and pressure of the wind features. The agreement between these analyses gives greater confidence in the ability to characterize year-to-year variability in the winds.

There are a number of periods during which there is an apparent connection (downward descent) between the easterly wind maximum around 0.01 hPa during equinox and the easterly wind maximum at 1 hPa at the following solstice. For example, see September to December 2003, March to June 2006, and a series of cycles beginning September 2012. For other periods, there is no evidence of a connection between the features at these two altitudes. Without further investigation into the processes driving the wind oscillation, it is not possible to determine whether this apparent spatial-temporal connection represents actual downward propagation.

Moss et al. (2016) found that the SAO winds at and above 81.5 km during March-April 2002 were much stronger than in the other years they observed. Figure 6 shows that the unusually strong winds are also seen in the winds derived from SABER around 0.01-0.004 hPa. The altitude of the easterly wind maximum is higher than average but not outside the range seen in other years. However, the combination of higher location of the easterly peak and strong maximum wind in the altitude range that can be observed by meteor radar sets this month apart. Winds at other levels during this period do not show any marked differences that would indicate that this perturbation is a response to unusual winds in the middle atmosphere below.

Previous observational studies (Burrage et al., 1996; Venkateswara Rao et al., 2012; de Wit et al., 2014) have noted that the magnitude of the SAO in the upper mesosphere has a strong variation in phase with the QBO in the stratosphere although there has been some debate about whether this modulation occurs only around the vernal equinox or throughout the year. The link between the phase of the QBO and the interannual variations in the satellite wind estimates in the upper stratosphere and mesosphere can be summarized by comparing the climatological winds for months with easterly and westerly phases of the QBO, as shown in Figure 8. The phase of the QBO is identified by the Singapore wind at 10 hPa and is evaluated for each month independently. As a result, the data in sequential months are not necessarily from the same sets of years.

The bottom panel of Figure 8 indicates where the differences are significant at the 95% level according to Student's t-test. Note that the significance is determined independently for each calendar month and pressure level. Overall, the differences in

401 magnitude are more likely to be significant during the periods after equinox (May-June
402 and October-November), which are periods of rapid change. The displacement in altitude
403 of the westerly equinox maxima (near 0.1 hPa during years when the QBO is westerly
404 and near 0.2 hPa during years when the QBO is easterly) is a prominent feature of the
405 difference plot. Using analysis from four years of wind observations, Ray et al. (1997)
406 noted several interannual variations in the stratopause SAO that followed the phase of the
407 QBO: weaker SAO westerlies and stronger SAO easterlies during the westerly QBO
408 phase and deeper descent of SAO westerly winds during the easterly QBO phase. The
409 current results (see also Figures 6 and 7) confirm these differences.

410 The stronger westerly winds near 0.1 hPa during the easterly QBO suggest
411 stronger wave driving by gravity waves and/or Kelvin waves. The westerly peaks are also
412 more clearly centered on the equinox periods during easterly QBO. Similar results are
413 obtained with the MLS dataset (not shown).

414 Figure 8 indicates that there is a relationship between the SAO and QBO but does
415 not indicate causality. It is most easily understood how the QBO could affect the SAO
416 through filtering of the waves that then dissipate and drive mean winds (Ray et al., 1997;
417 Garcia and Sassi, 1999; Peña-Ortiz et al., 2012). However, examination of the month-by-
418 month equatorial winds derived here does not lead to a straightforward explanation. For
419 any given month, the QBO winds between the levels of 70 and 3 hPa include both
420 easterly and westerly winds that cover similar ranges of values (roughly peak easterly
421 winds of -20 to -30 m/s and peak westerly winds of 10 to 15 m/s). We were not able to
422 identify a clear QBO dependence of the predicted critical level filtering based on the peak
423 winds encountered in a vertical column in the lower to middle stratosphere. It may be, as

424 suggested by wave calculations by Ray et al. (1997) and simulations by Peña-Ortiz et al.
425 (2012), that the key differences in wave forcing occur away from the equator.
426 It is also possible that the causality is in the opposite direction; i.e., that the SAO,
427 especially at its lower reaches in the upper stratosphere, has an impact on the QBO. For
428 example, the stronger easterly winds near the stratopause in the westerly phase of the
429 QBO can contribute to seeding the wind shear in the upper stratosphere that is associated
430 with the shift from the westerly to the easterly phase of the QBO. This mechanism is also
431 not straightforward due to the time delay of several months needed for the QBO to
432 propagate downward from the lower limit of the SAO to the 10 hPa level. The slow
433 downward propagation of the QBO would imply a lag in the signal between the upper
434 stratosphere SAO and the 10 hPa QBO but no lag was used in assigning the winds in
435 Figure 8 to easterly or westerly QBO phases.
436
437 **5. Conclusions**
438 This study shows the climatology and interannual variability of the SAO in
439 middle atmosphere zonal wind from 100 to 0.004 hPa. The winds are derived from
440 almost 15 years of geopotential height data from TIMED/SABER and more than 12 years
441 of data from Aura/MLS. This analysis fills in the current gap in continuous equatorial
442 wind measurements between 10 and 0.01 hPa; equatorial winds calculated in current
443 reanalysis products (e.g., Rienecker et al., 2012; Coy et al., 2016) cover only part of this
444 range. Comparisons of the zonally averaged winds with observed radiosonde winds at
445 Singapore (1°N, 90-10 hPa) and with meteor radar winds at Ascension Island (8°S, 81.5-

446 84 km) indicate that winds derived from both satellite datasets capture the mean and the
447 seasonal and interannual variability.
448 The primary contributions that these satellite wind analyses can make to the
449 investigation of the SAO are 1) long data records with no gaps in coverage and 2)
450 continuous vertical coverage through the depth of the middle atmosphere. The vertical
451 range covers the transition from QBO dominance in the lower to middle stratosphere to
452 SAO dominance in the upper stratosphere and the transition from the stratopause SAO to
453 the mesopause SAO. As discussed in Section 2, a primary concern is possible
454 contamination of the SABER time-mean zonal-mean fields by the migrating diurnal tide
455 near the mesopause. Although not considered in the present study, both SABER and
456 MLS can also give information about waves that have large enough horizontal and
457 vertical scales to be resolved in the observations; these include fast Kelvin waves, a
458 subset of gravity waves and, for SABER, tides with diurnal periods.
459 Another aspect of the SAO that can be seen in these wind derivations is its
460 latitudinal structure. Through most of the mesosphere, the latitude structure of the SAO
461 does not show maxima at the equator that are isolated in latitude but rather indicates that
462 the tropical winds during both easterly and westerly phases are part of a large scale
463 structure with downward descent in time.
464 Earlier investigations (Burrage et al., 1996; deWit et al., 2013) found that there is
465 a large variation of the SAO in the upper mesosphere with the phase of the QBO in
466 stratospheric winds. Note that the satellite analyses of Burrage et al. (1996), which used
467 daytime only data, may have some contamination from the large semiannual and QBO
468 variations in the amplitude of the migrating diurnal tide. The results presented here

469 greatly expand the information available by showing the SAO over a broad vertical range
470 using two long continuous data records that have day and night observations. These show
471 convincingly that the equatorial mesospheric winds at all times of year vary depending on
472 the QBO phase.

473 Although an observed relationship between the QBO and the SAO has been seen
474 previously, the explanation is still incomplete. Peña-Ortiz et al (2012) showed that a
475 comprehensive whole atmosphere model with an interactively generated QBO could
476 reproduce a link between the QBO and the mesospheric SAO. They found that forcing by
477 both small-scale (parameterized) gravity waves and resolved waves contributed to the
478 variability. The extent to which the SAO varied with the phase of the QBO was larger in
479 their model simulations than in the current observational analysis.

480 There are several mechanisms by which the QBO could alter the SAO forcing in
481 the mesosphere. Possibilities are 1) the QBO winds selectively filter and absorb upward
482 propagating large-scale equatorial waves such as Kelvin waves (Garcia and Sassi, 1999);
483 2) the QBO filters small-scale gravity waves in the tropical region; or 3) the QBO winds
484 affect midlatitude dynamics in the winter hemisphere that then affect the driving of the
485 SAO winds by large-scale advection. These mechanisms are not independent due to the
486 interaction of wave propagation and dissipation with the background wind. Although
487 details and mechanisms involved in the interaction between the QBO and SAO are still
488 not resolved, the middle atmosphere winds derived here provide a powerful new set of
489 observations that can be used for guiding further investigation.
490

491 **Acknowledgements**

The National Center for Atmospheric Research is sponsored by the US National Science Foundation. Additional support was provided by the US National Aeronautics and Space Administration (NASA) Grant NNX14AD83G. The authors thank Dave Ortland, Bill Randel, and Dan Marsh for helpful comments on the manuscript and Tom Marshall for providing reprocessed SABER Level 2A data for 2015-2016.

NASA supports the TIMED and Aura satellites and their instruments; retrieved profile data are freely available. Version 2.0 profile data from TIMED/SABER are available from http://saber.gats-inc.com. Version 4.2 geopotential height profile data from MLS are available from http://disc.sci.gsfc.nasa.gov/Aura/data-holdings/MLS/index.shtml.

Monthly averaged radiosonde zonal wind data measured at Singapore have been compiled by the Freie Universität Berlin and are available from http://www.geo.fu-berlin.de/en/met/ag/strat/produkte/qbo/.

Data for the monthly mean zonal wind estimates presented in this paper can be obtained from the lead author.

References

Baldwin, M. P., and L. J. Gray, 2005: Tropical stratospheric zonal winds in ECMWF ERA-40 reanalysis, rocketsonde data, and rawinsonde data, *Geophys. Res. Lett.*, 32, L09806, doi:10.1029/2004GL022328.

Burrage, M. D., M. E. Hagan, W. R. Skinner, D. L. Wu, and P. B. Hays, 1995a: Long-term variability in the solar diurnal tide observed by HRDI and simulated by the GSWM. *Geophys. Res. Lett.*, 22, 2641-2644.

Burrage, M. D., Wu, D. L., Skinner, W. R., Ortland, D. A., and Hays, P. B., 1995b: Latitude and seasonal dependence of the semidiurnal tide observed by the high-resolution Doppler imager. *J. Geophys. Res.*, 100, 11313–11321.

Burrage, M. D., R. A. Vincent, H. G. Mayr, W. R. Skinner, N. F. Arnold, and P. B. Hays, 1996: Long-term variability in the equatorial middle atmosphere zonal wind. *J. Geophys. Res.,* 101, 12,847–12,854, doi:10.1029/96JD00575.

Coy, L., K. Wargan, A. M. Molod, W. R. McCarty, and S. Pawson, 2016: Structure and dynamics of the quasi-biennial oscillation in MERRA-2. *J. Clim.*, 29, 5339-5354, doi: 10.1175/JCLI-D-15-0809.1

Davis, R. N., J. Du, A. K. Smith, W. E. Ward, and N. J. Mitchell, 2013: The diurnal and semidiurnal tides over Ascension Island (8°S, 14°W) and their interaction with the stratospheric QBO: studies with meteor radar, eCMAM and WACCM. *Atmos. Chem. Phys.*, 13, 9543–9564, doi:10.5194/acp-13-9543-2013.

deWit, R. J., R. E. Hibbins, P. J. Espy, and N. J. Mitchell, 2013: Interannual variability of mesopause zonal winds over Ascension Island: Coupling to the stratospheric QBO. *J. Geophys. Res.*, 118, 12,052–12,060, doi:10.1002/2013JD020203.

531 Garcia, R. R., T. J. Dunkerton, R. S. Lieberman, and R. A. Vincent, 1997: Climatology of
532 the semiannual oscillation of the tropical middle atmosphere. *J. Geophys. Res.*,
533 102, 26,019–26,032, doi:10.1029/97JD00207.
534 Garcia, R. R. and F. Sassi, 1999: Modulation of the mesospheric semiannual oscillation
535 by the quasibiennial oscillation. *Earth Planets Space*, 51, 563-569.
536 Hamilton, K., A. Hertzog, F. Vial, and G. Stenchikov, 2004: Longitudinal Variation of
537 the Stratospheric Quasi-Biennial Oscillation, J. Atmos. Sci., 61, 383-402, doi:
538 http://dx.doi.org/10.1175/1520-0469(2004)061<0383:LVOTSQ>2.0.CO;2.
539 Kawatani, Y., K. Hamilton, K. Miyazaki, M. Fujiwara, and J. A. Anstey, 2016:
540 Representation of the tropical stratospheric zonal wind in global atmospheric
541 reanalyses. *Atmos. Chem. Phys.*, 16, 6681–6699, doi:10.5194/acp-16-6681-2016
542 Kishore Kumar, G., K. Kishore Kumar, W. Singer, C. Zülicke, S. Gurubaran, G.
543 Baumgarten, G. Ramkumar, S. Sathishkumar, and M. Rapp, 2014: Mesosphere
544 and lower thermosphere zonal wind variations over low latitudes: Relation to
545 local stratospheric zonal winds and global circulation anomalies. *J. Geophys.*
546 *Res.*, 119, 5913–5927, doi:10.1002/2014JD021610.
547 Moss, A. C., C. J. Wright, R. N. Davis, and N. J. Mitchell, 2016: Gravity-wave
548 momentum fluxes in the mesosphere over Ascension Island (8° S, 14° W) and the
549 anomalous zonal winds of the semi-annual oscillation in 2002. *Ann. Geophys.*, 34,
550 323-330, doi:10.5194/angeo-34-323-2016.
551 Naujokat, B., 1986: An update of the observed quasi-biennial oscillation of the
552 stratospheric winds over the tropics. *J. Atmos. Sci.*, 43, 1873-1877.
553 Niciejewski, R., Q. Wu, W. Skinner, D. Gell, M. Cooper, A. Marshall, T. Killeen, S.

554 Solomon, and D. Ortland, 2006: TIMED Doppler Interferometer on the
555 Thermosphere Ionosphere Mesosphere Energetics and Dynamics satellite: Data
556 product overview. *J. Geophys. Res.*, 111, A11S90, doi:10.1029/2005JA011513.
557 Peña-Ortiz, C., H. Schmidt, M. A. Giorgetta, and M. Keller, 2010: QBO modulation of
558 the semiannual oscillation in MAECHAM5 and HAMMONIA, *J. Geophys. Res.*,
559 115, D21106, doi:10.1029/2010JD013898.
560 Randel, W. J., 1987: The evaluation of wind from geopotential height data in the
561 stratosphere. *J. Atmos. Sci.*, 44, 3097-3120.
562 Randel, W., and collaborators, 2004: The SPARC intercomparison of middle-atmosphere
563 climatologies, *J. Clim.*, 17, 986-1003.
564 Ray, E. A., M. J. Alexander, and J. R. Holton, 1998: An analysis of the structure and
565 forcing of the equatorial semiannual oscillation in zonal wind, *J. Geophys. Res.*,
566 103(D2), 1759–1774, doi:10.1029/97JD02679.
567 Richter, J. H., and R. R. Garcia, 2006: On the forcing of the mesospheric semi-annual
568 oscillation in the Whole Atmosphere Community Climate Model. *Geophys. Res.*
569 *Lett.*, 33, L01806, doi:10.1029/2005GL024378.
570 Rienecker, M. M., and collaborators, 2011: MERRA: NASA's modern-era retrospective
571 analysis for research and applications. *J. Clim.*, 24, 3624–3648,
572 doi:10.1175/JCLI-D-11-00015.1.
573 Salby, M. L., 1982a: Sampling theory for asynoptic satellite observations. Part I: Space-
574 time spectra, resolution, and aliasing. *J. Atmos. Sci.*, 39, 2577-2600,
575 doi:10.1175/1520-0469(1982)039<2577:STFASO>2.0.CO;2
576 Salby, M. L., 1982b: Sampling theory for asynoptic satellite observations. Part II: Fast

577 Fourier synoptic mapping, *J. Atmos. Sci.*, 39, 2601-2614, doi:10.1175/1520-
578 0469(1982)039<2601:STFASO>2.0.CO;2
579 Schwartz, M. J., and Coauthors, 2008: Validation of the Aura Microwave Limb Sounder
580 temperature and geopotential height measurements, *J. Geophys. Res*., **113**,
581 D15S11, doi:10.1029/2007JD008783.
582 Venkateswara Rao, N., T. Tsuda, D. M. Riggin, S. Gurubaran, I. M. Reid, and R. A.
583 Vincent, 2012: Long-term variability of mean winds in the mesosphere and lower
584 thermosphere at low latitudes. *J. Geophys. Res.*, 117, A10312,
585 doi:10.1029/2012JA017850.
586 Wu, Q., D. A. Ortland, T. L. Killeen, R. G. Roble, M. E. Hagan, H.-L. Liu, S. C.
587 Solomon, J. Xu, W. R. Skinner, and R. J. Niciejewski, 2008: Global distribution
588 and interannual variations of mesospheric and lower thermospheric neutral wind
589 diurnal tide: 1. Migrating tide. *J. Geophys. Res.*, 113, A05308,
590 doi:10.1029/2007JA012542.

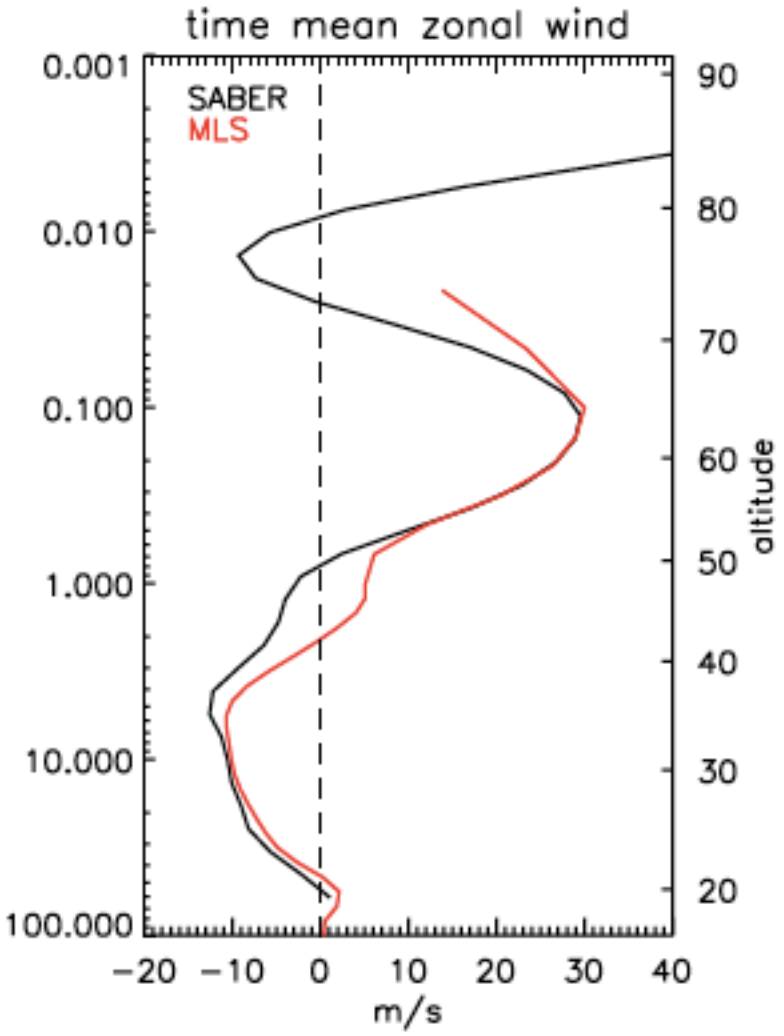

591

592 **Figure 1**: Time mean zonal mean zonal wind at the equator derived from SABER (black)

593 and MLS (red).

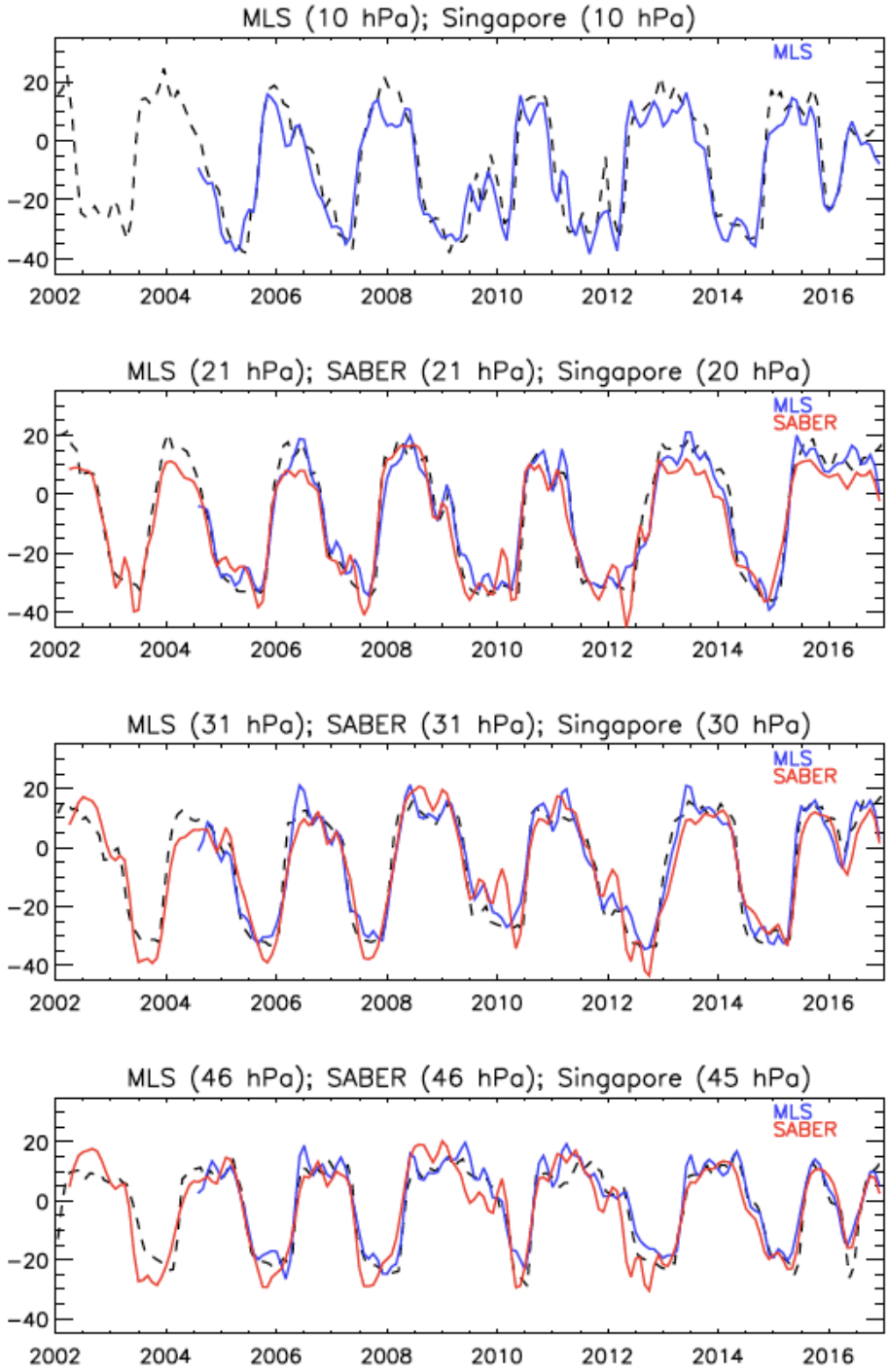

Figure 2: Time series of monthly mean zonal mean zonal wind at the equator derived from SABER (red lines), MLS (blue lines) and from radiosondes at Singapore (1°N; dashed black lines) at levels near 10, 20, 30, and 45 hPa.

598

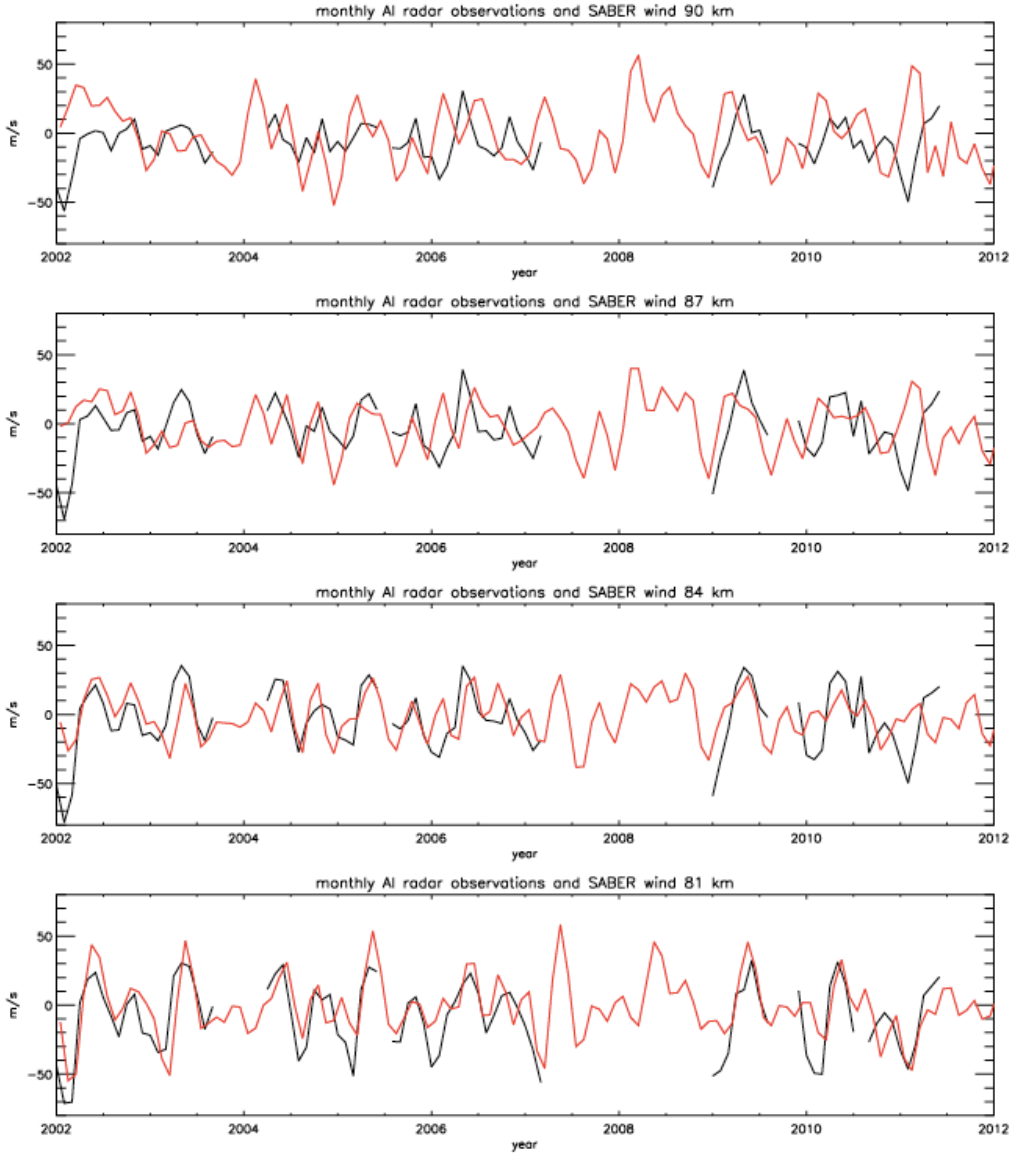

599

600 **Figure 3**: Monthly mean zonal wind from meteor radar at Ascension Island (8°S), shown
601 in black, at four altitude levels. Red curves show wind derived from SABER at the same
602 latitude and altitudes (red). As discussed in the text, the time mean wind has been
603 removed from SABER.

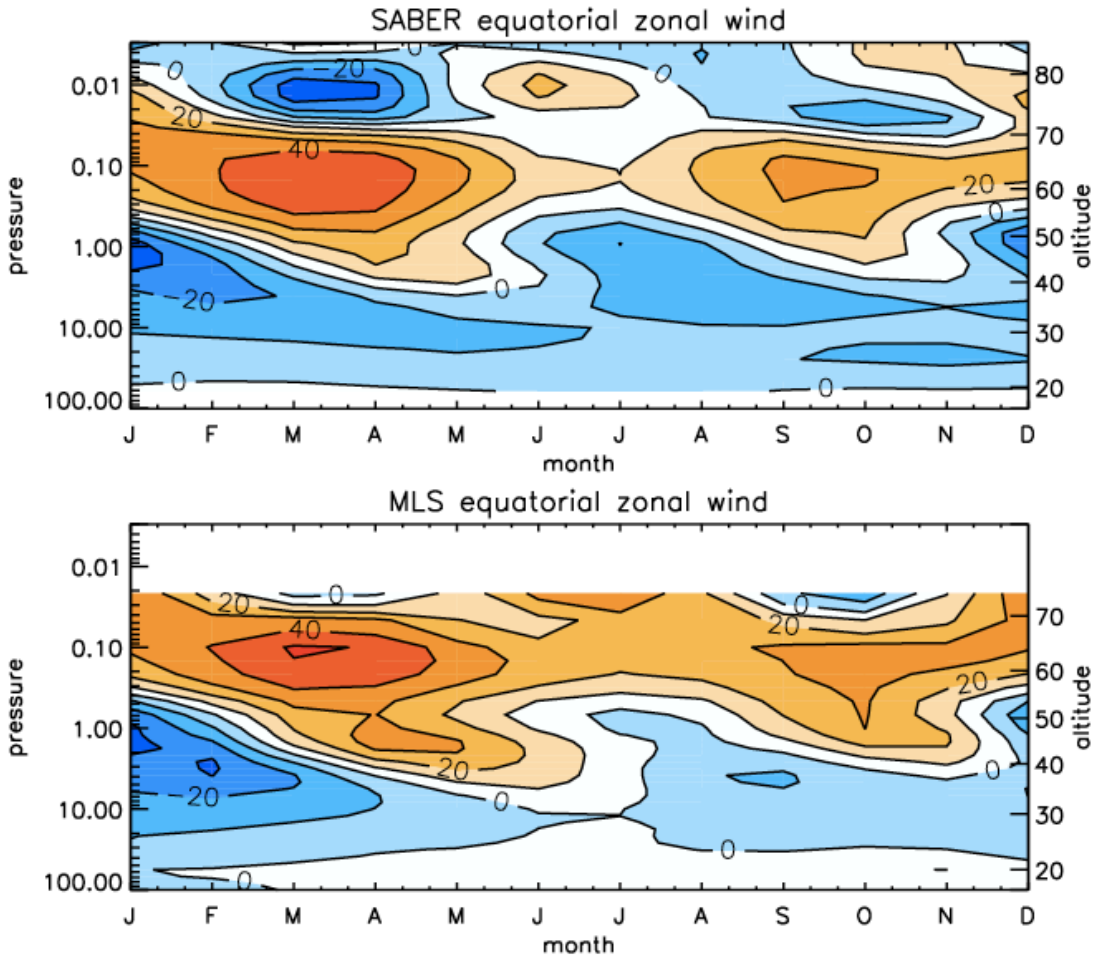

604

605 **Figure 4**: Multiyear average of monthly equatorial wind from SABER (top) and MLS

606 (bottom).

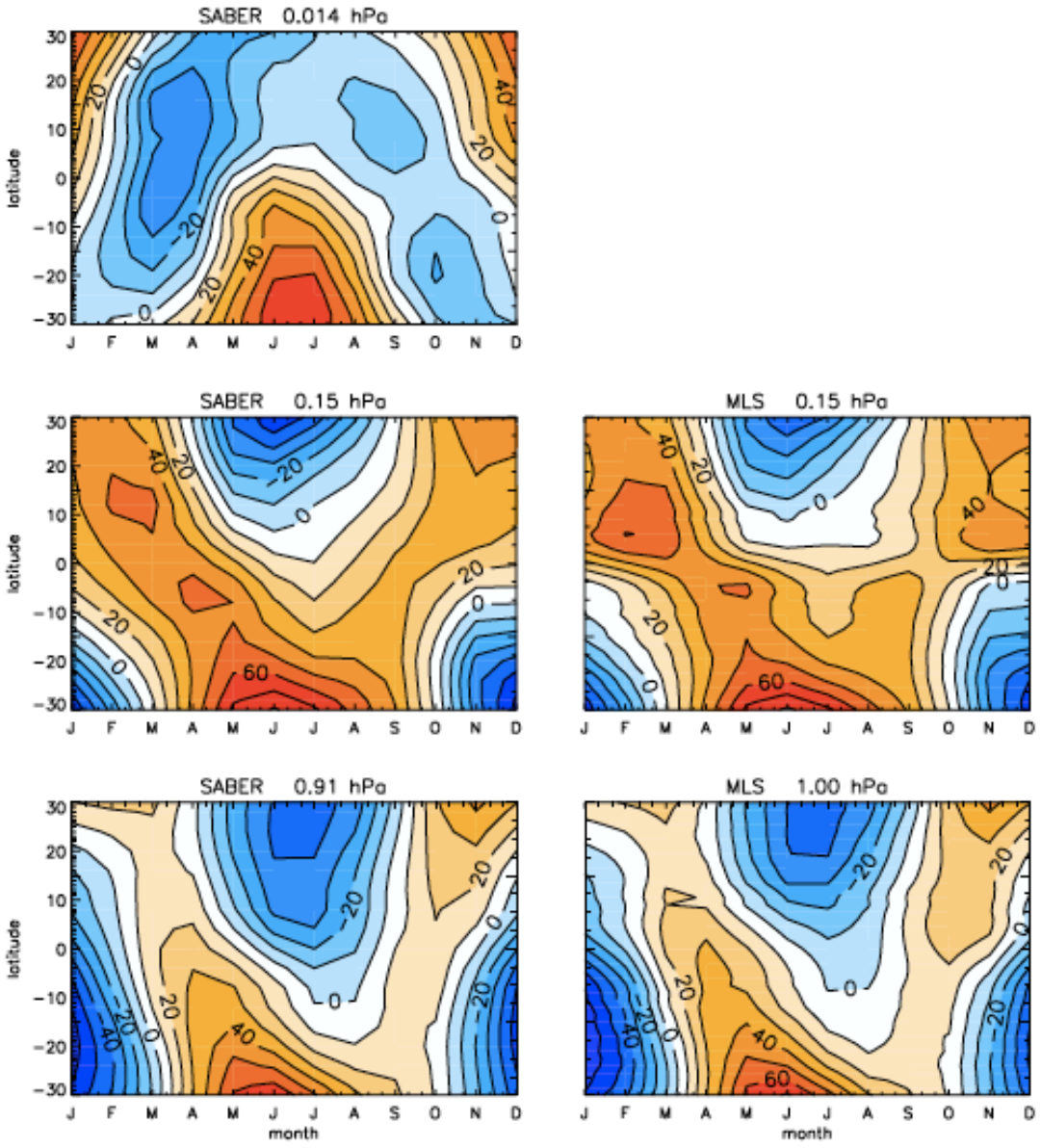

607

608 **Figure 5**: Latitude x month sections of zonal wind from SABER at three pressure levels

609 (left) and MLS at two levels (right).

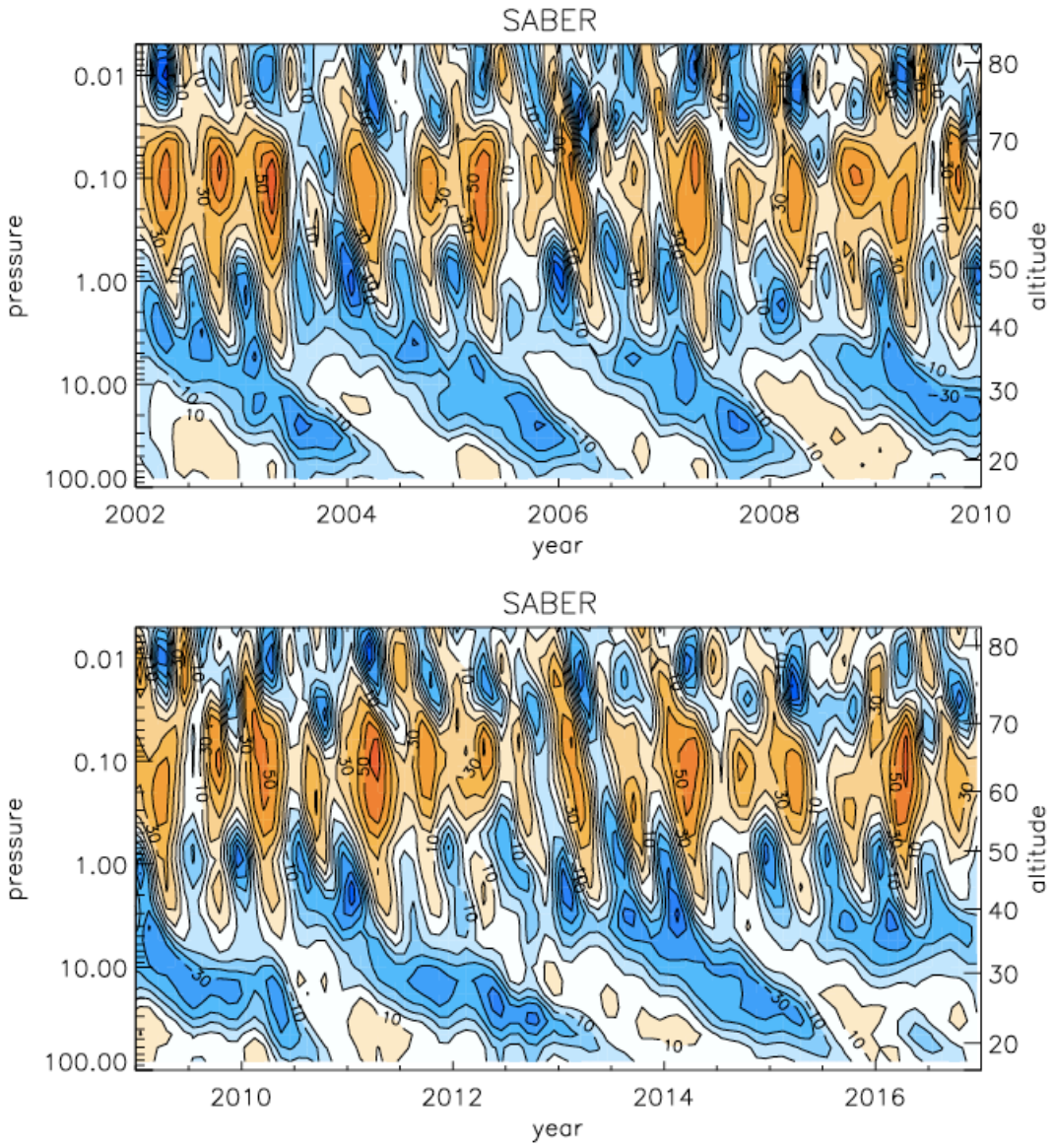

610

611 **Figure 6**: Timeseries of SABER monthly mean wind at the equator.

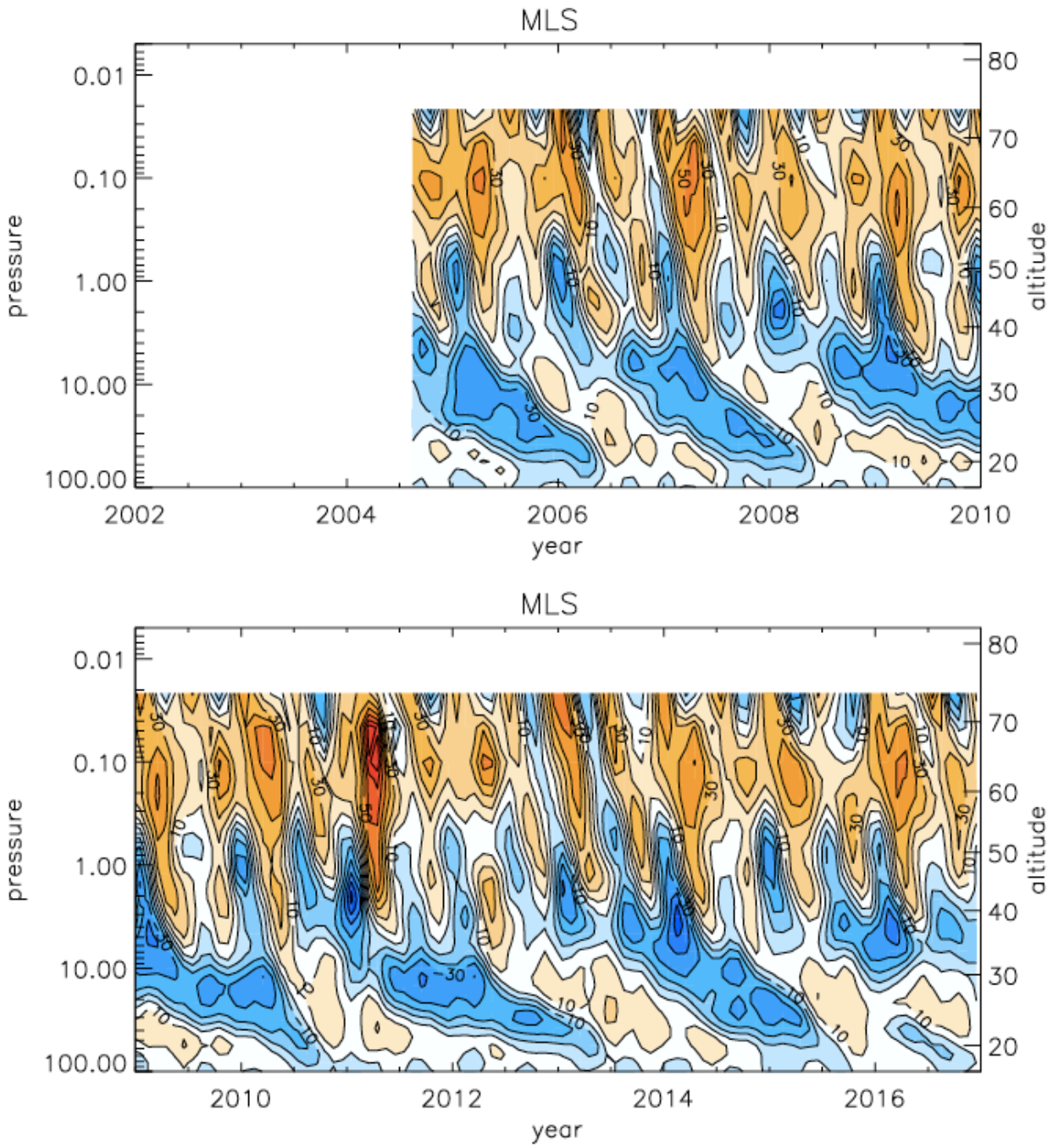

612

613 **Figure 7**: Timeseries of MLS monthly mean wind at the equator.

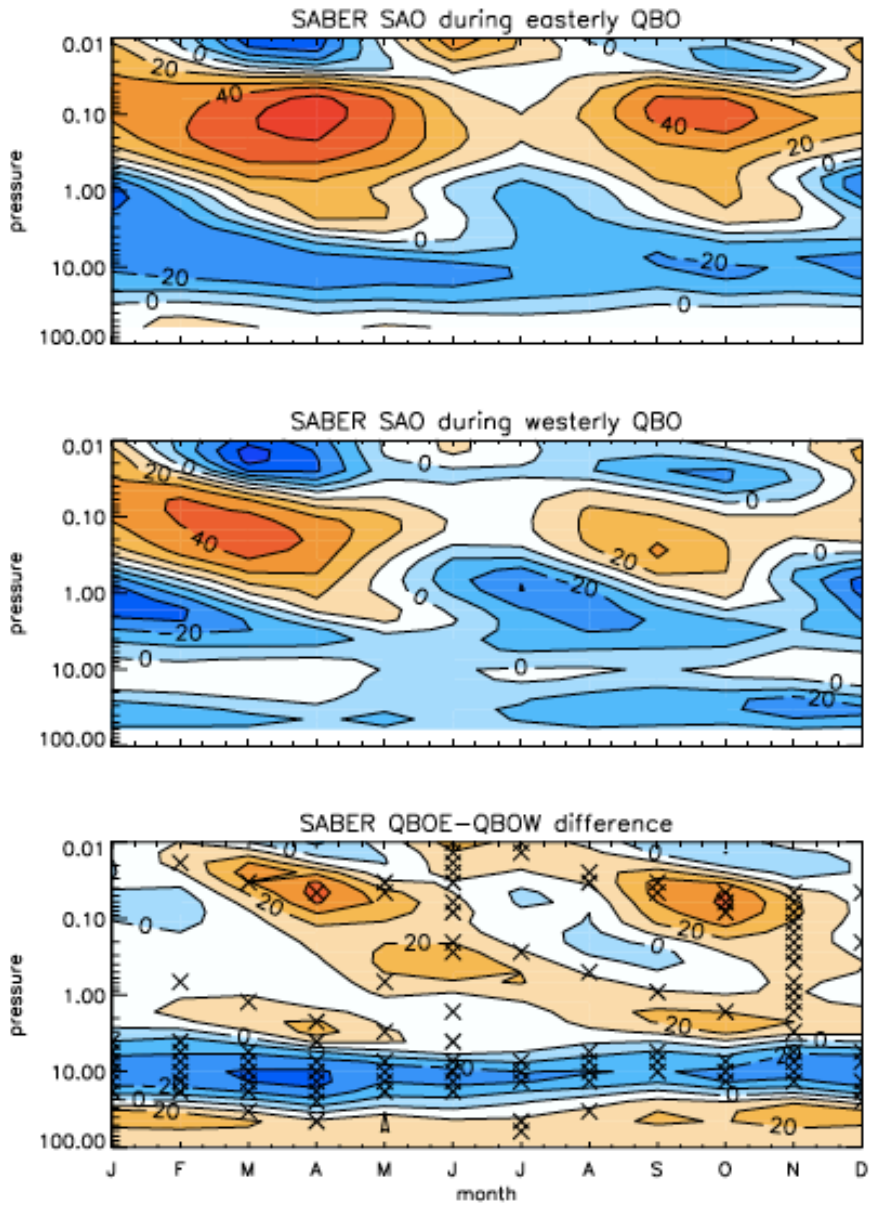

614

615

616 **Figure 8**: Climatological variation of monthly mean equatorial wind derived from

617 SABER, as in Figure 4b except separated by the phase of the QBO in Singapore winds at

618 10 hPa. Top: winds when the QBO is easterly; middle: winds when the QBO is westerly;

619 bottom: difference. The crosses indicate where the differences are significant at the 95%

620 level.